techniques, with additional complications due to the Na night-sky lines, the continuum spectrum of Io, and the water absorption features.
12. F. Bagenal, *J. Geophys. Res.* **99**, 11043 (1994).
13. To examine the long-term behavior of the plasma torus intensities, we removed short-term periodic modulations in the S^+ emission. The two observed modulations in the data occur at periods of 9.925 hours (the System III rotational period of Jupiter) and 10.214 hours {an unexplained modulation termed "System IV" [B. R. Sandel and A. J. Dessler, *ibid.* **93**, 5487 (1988)]} [M. E. Brown, *ibid.* **100**, 21683 (1995)]. The measured intensities are divided by the sliding-average of the modulation at these periods to remove the variations of about 30 and 40% for System III and IV, respectively. The emission intensity of S^+ is proportional to the product of the electron and ionized S densities, (approximately proportional to the square of the S^+ density), as the emission is due to the electron impact excitation of the S. Analysis of the emission intensities from the neutral Na cloud suffers the complication that the emission seen is from the resonant scattering of sunlight; the emission intensity thus depends on the received solar flux at the wavelength of the atomic transition, and therefore, on the heliocentric velocity of the Na atoms [J. T. Bergstralh, J. W. Young, D. L. Matson, T. V. Johnson, *Astrophys. J.* **211**, L51 (1977); R. A. Brown and Y. L. Yung, in *Jupiter*, T. Gehrels, Ed. (Univ. of Arizona Press, Tucson, 1976), pp. 1102–1145]. This effect is dependent mostly on Io's orbital phase, so we correct by removing the sliding-average modulation of the data at Io's orbital period. The total modulation by Io phase is 50%.
14. We estimated the total mass increase in the plasma torus by summing all emission along the slit and taking the square root, as the emission intensity is proportional to the product of the ion density and the electron density, which we assume scale together. Figure 2 appears to imply an even larger change in mass only because of the structural changes that occur in the torus at the same time.
15. An alternative scenario might be envisioned where the increase in mass of the neutral Na cloud is caused by an increase in the Na lifetime caused, for example, by a decrease in the electron temperature. We reject this hypothesis for two reasons: (i) Observations of the plasma torus, while not directly sensitive to electron temperature, show no change in the plasma torus mass, ion temperature, or rotation velocity at the start of the neutral Na cloud perturbation, and (ii) the increase in mass of the plasma torus shows that for S, at least, the supply increases precisely when the Na mass increases, strongly suggesting that the Na mass increase is caused by a Na supply increase.
16. C. B. Pilcher, J. H. Fertel, J. S. Morgan, *Astrophys. J.* **207**, 181 (1980); A. J. Dessler and B. R. Sandel, *Geophys. Res. Lett.* **19**, 2099 (1992); N. M. Schneider and J. T. Trauger, *Astrophys. J.* **450**, 450 (1995).
17. D. D. Barbosa and M. G. Kivelson, *Geophys. Res. Lett.* **10**, 210 (1983).
18. The lack of a shift on the duskside is unexpected. If the electric field operates uniformly across the magnetic field both sides should shift equally. The exclusively dawnside shift suggests that the electric field variations occur only on the dawn, explaining these data and also the sporadic dawnside shifts observed in imaging data (*16*).
19. T. W. Hill, *J. Geophys. Res.* **84**, 6554 (1979). Voyager measurements show that $L_H \sim 20\ R_J$.
20. We are indebted to A. J. Dessler for the analogy to terrestrial equatorial currents and for the suggestion of the form of the relationship between an increasing plasma outflow and an increasing electric field.
21. The data were grouped into four groups for determination of the emission peak. The groups correspond to (in order of faintest to brightest) preoutburst (days 580 through 689), increasing phase of outburst (days 690 through 700), declining phase of outburst (days 723 through 750), and peak of outburst (days 700 through 722) periods. The fractional torus shift is defined as $(p_{dawn} - p_{dusk})/(p_{dawn} + p_{dusk})$, where p_{dawn} and p_{dusk} are the position of the peak of plasma torus intensity on the dawn and dusk sides, respectively. As above, the relative density is estimated by the square root of the total intensity integrated along the spectral slit. The theoretical curves are calculated assuming zero electric field for a zero mass plasma torus and by forcing the curves to go through the equilibrium mass point (relative torus mass of 1.0).
22. The models of the behavior of the neutral cloud and magnetosphere mass are based on the zero-dimensional models of T. S. Huang and G. L. Siscoe [*J. Geophys. Res.* **91**, 10163 (1986)]. For the supply-limited case, supply to the neutral cloud is proportional to the square root of the plasma density, and diffusive loss from the magnetosphere is proportional to the plasma density. For the loss-limited case, supply to the neutral cloud is proportional to the plasma density, and loss from the magnetosphere is proportional to the fourth power of the plasma density. For both cases, model input parameters are adjusted to yield a steady-state plasma lifetime of 30 days and a neutral lifetime of 20 hours.
23. Direct imaging of a new plume at the time of the outburst would provide conclusive proof of this hypothesis, but the capability of obtaining such an image was not available at the time of these observations. Ground-based infrared observations are able to monitor hotspot activity on Io, but we have no reason to expect that these are associated with plumes on Io, nor were any observations obtained during the outburst [G. J. Veeder, D. L. Matson, T. V. Johnson, D. L. Blaney, J. D. Goguen, *ibid.* **99**, 17095 (1994)].
24. See, for example, E. Lellouch, *Icarus* **124**, 1 (1996).
25. W. H. Smyth and M. R. Combi, *Astrophys. J.* **328**, 888 (1988).
26. D. F. Strobel, in (*5*), pp. 183–195.
27. We benefited greatly from conversations with A. J. Dessler, T. W. Hill, M. A. McGrath, E. J. Moyer, and D. H. Pontius. This research would not have been begun without a generous seed grant from the California Space Institute and would not have proceeded without the reliable help of A. Misch and the other staff at Lick Observatory.

6 May 1997; accepted 12 August 1997

Organics and Other Molecules in the Surfaces of Callisto and Ganymede

T. B. McCord,* R. W. Carlson, W. D. Smythe, G. B. Hansen, R. N. Clark, C. A. Hibbitts, F. P. Fanale, J. C. Granahan, M. Segura, D. L. Matson, T. V. Johnson, P. D. Martin

Five absorption features are reported at wavelengths of 3.4, 3.88, 4.05, 4.25, and 4.57 micrometers in the surface materials of the Galilean satellites Callisto and Ganymede from analysis of reflectance spectra returned by the Galileo mission near-infrared mapping spectrometer. Candidate materials include CO_2, organic materials (such as tholins containing C≡N and C–H), SO_2, and compounds containing an SH-functional group; CO_2, SO_2, and perhaps cyanogen [$(CN)_2$] may be present within the surface material itself as collections of a few molecules each. The spectra indicate that the primary surface constituents are water ice and hydrated minerals.

The four largest satellites of Jupiter, called the Galilean satellites after their discoverer, are a mini solar system. They are about moon-sized to larger than Mercury, and the innermost satellite, Io, is the most volcanically active body in the solar system. Europa, the second Galilean satellite from Jupiter, has a dense core and an ice crust that may be underlain by a liquid water ocean. Ganymede, the third Galilean satellite, is also differentiated, with scars from giant impacts but clearly showing essentially complete resurfacing. Finally, Callisto, the fourth satellite, appears heavily cratered and undifferentiated, thus perhaps preserving evidence of its early history (*1*). The Galilean satellites are located in the temperature region of the solar system where water ice and other volatiles become stable over the age of the solar system (*2*). The composition and chemistry of the surfaces of these objects is of interest because they provide clues to the origin of our solar system and because they contain water ice and may contain organic molecules that are essential for the initiation of life.

The NASA Galileo spacecraft carried the near-infrared mapping spectrometer (NIMS) (*3*) into orbit around Jupiter on 7 December 1995, and the NIMS started spectrometric observations of the Galilean satellites in June 1996 (*4*, *5*). The NIMS covers the wavelength range 0.7 to 5.2 μm with up to 408 spectral channels and a resolving power of 40 to 200 ($\Delta\lambda/\lambda$, where λ is wavelength). The instrument's instantaneous field of view is 0.5 mrad, giving a spatial resolution (pixel size) of, for example, 5 km at a distance of 10,000 km. The

T. B. McCord, G. B. Hansen, C. A. Hibbitts, F. P. Fanale, P. D. Martin, Hawaii Institute of Geophysics and Planetology, University of Hawaii, Honolulu, HI 96822, USA.
R. W. Carlson, W. D. Smythe, M. Segura, D. L. Matson, T. V. Johnson, Jet Propulsion Laboratory, Pasadena, CA 91109, USA.
R. N. Clark, U.S. Geological Survey, Denver, CO 80225–0046, USA.
J. C. Granahan, Science and Technology International, Incorporated, Honolulu, HI 56813, USA.

*To whom correspondence should be addressed. E-mail: tom@kahana.pgd.hawaii.edu

data are encoded into 10-bit data numbers, formatted, and usually written to the spacecraft tape recorder for later transmission to Earth.

Water ice spectral features dominate the NIMS reflectance spectra for Callisto and Ganymede (Fig. 1). The strong absorption near 3 μm is the fundamental O–H stretching transition active in water ice as well as in hydrated and hydroxylated minerals. All other bands evident in the 1- to 3-μm region are due to combination and overtone transitions in water ice for which there is not complete agreement on the individual band assignments (*6*). These include bands centered at 1.04, 1.25, 1.5, and 2 μm, and a temperature-sensitive band at 1.65 μm, at the edge of the 1.5-μm feature (*7*). The presence of water ice features in the spectrum of the three icy Galilean satellites of Jupiter was known from ground-based telescope observations (*8*). Water ice is strongly absorbing longward of 2.5 μm and is responsible for much of the low reflectance in this region for Ganymede. For Callisto, the spectrum longward of 2.5 μm is not as depressed and is due almost entirely to non–water-ice components. The features of water ice longward of 3 μm, although strong, are also broad, therefore allowing one to discern non-ice features better than in the region shortward of 3 μm even when water ice is present. Thus, our initial analysis emphasized this longer wavelength spectral region.

Averaged spectra (Fig. 1) were calculated to enhance the detection of weak spectral features in the region longward of 3 μm. A 4.25-μm absorption is well defined and several other weaker absorptions near 3.88, 4.05, and 4.57 μm can be seen in the spectra of Callisto. These features also occur in the Ganymede spectra, although they are generally weaker by about a factor of 2. The presence of the same bands suggests the same compositions and thus common origins or processes on both Callisto and Ganymede.

A survey of the NIMS data for Callisto and Ganymede shows that, in general, the non-ice spectral absorptions described so far vary in strength with location in different ways for each of these spectral features, indicating that the absorptions are each due to a different material (*5*). For example, the 4.25-μm absorption on Callisto is associated with many, but not all, bright "fresh" impact features and with the center of the Asgard basin, whereas the 4.05-μm absorption is not closely associated with these features. Also, the 4.25-μm absorption is stronger on the trailing side of Callisto, whereas the 4.05- and 4.57-μm absorptions are stronger on the leading side. In general, the absorption distributions are complex.

We eliminated many candidate materials from consideration for explaining the absorptions by noting that (i) they do not have absorptions similar to any of those found in the NIMS data, or (ii) they also have other strong absorptions not apparent in the NIMS spectra. For example, in the case of salts, nitrates have too many strong bands in the 3- to 5-μm region, which are not evident here, and carbonates do not have bands that match the bands found. Sulfates and other sulfur-oxygen compounds (for example, sulfites and sulfones) could be candidates for the 4.57-μm absorption, but these materials usually also have bands at other wavelengths that do not appear in the NIMS data. Many databases were searched to identify candidate materials for these absorptions (*9*–*11*), including those containing minerals, organics, and volatiles in both gaseous and solid states.

An obvious candidate for the 4.25-μm absorption feature (Fig. 1) is CO_2. Carbon dioxide has a well-known fundamental absorption band near 4.25 μm and is the obscuring gas in Earth's atmosphere that prevents ground-based telescopic observations of the Galilean satellites in this general spectral region. The CO_2 band strength, width, and position vary with phase, temperature, and molecular environment, for example, a pure CO_2 crystal structure compared with CO_2 in solution with another solid material. A slab absorption radiative transfer model (Beer's law with only the imaginary part of the CO_2 index of refraction) was used to calculate spectra for comparison with the 4.25-μm absorption (Fig. 2A). A pure frost model was not used because exposed CO_2 frost or ice would not be stable for geologic time at the surface temperatures (140 to 160 K maximum) of Ganymede or Callisto. The band shape requires that the CO_2 must be in a form that does not allow molecular rotations (such as a pure solid or located in the tightly confined crystalline structure of another material) because of the absence of broad absorption bands due to the coupling of vibrational and rotational energy levels such as are found in the vibration-rotation bands in gases (*12*). The ν_3 (4.25-μm) band in gaseous CO_2, in fact, has no strong absorption in the center of the band where the rotational energy difference is zero; rather, the absorption is concentrated in broad bands covering several tenths of a micrometer on either side of the vibrational wavelength. On the other hand, in a condensed phase this vibrational mode is so strong that a photon needs to encounter only about 350 molecules to have a 1/*e* probability of being absorbed, implying a column density of about 3×10^{17} molecules per square centimeter to produce this absorption.

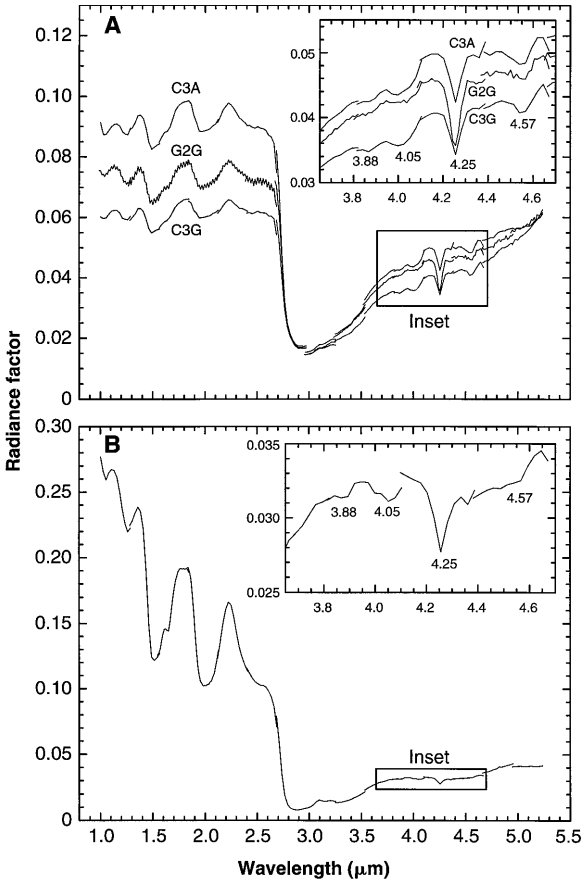

Fig. 1. NIMS spectra for (**A**) Callisto and (**B**) Ganymede. The ordinate for each plot is radiance factor (the ratio of the measured radiance to that of a Lambertian surface illuminated and viewed from the normal direction). Each of the spectra is an average of all of the spectra in an observation. For Callisto (A) the averaged areas are G2-GLOBAL (G2G, 600 pixels, 230°W to 360°W), C3-GLOBAL (C3G, 3000 pixels, 90°W to 190°W), and C3-ARINGS [C3A, 1500 pixels from a local (104 km^2) observation]. The inset graph is an enlargement of the wavelength region where the four absorptions were found. For Ganymede (B), the spectrum is an average of 3000 pixels from a global observation covering 110°W to 230°W. The inset shows enlargements of the four absorptions. The nonsystematic errors are a few line widths in size.

The small shift in wavelength of the absorption from that of crystalline CO_2, required to match the Callisto spectrum, indicates that the CO_2 may be dispersed in another material. Bulk CO_2 ice or frost could exist only if there was a continuous source to balance the evaporative loss, perhaps by outgassing from below or by active processes in the surface. More likely, the CO_2 is present in the surface material concentrated in deposits of one or a few molecules each so that the molecules are more tightly constrained than in crystalline CO_2 ice [shorter wavelength absorption (Fig. 2A)]. The CO_2 could be dissolved in water ice (for example, in a clathrate structure, mixed in amorphous ice or trapped in grain boundaries and dislocations), which does not affect the stability of the water ice (*13*), or in non–water-ice materials. We have observed that the 4.25-μm absorption can be equally strong in regions with widely different amounts of water ice. Johnson and Jesser (*14*) have suggested such a model to explain reported O_2 and O_3 absorptions in Ganymede spectra (*15*). In their model, defects and voids are formed in the crystal structure by particle radiation from the jovian magnetosphere, and species, perhaps generated by the radiation, accumulate in the voids. They suggest that O_2 and O_3 deposits are formed by the dissociation of H_2O and diffusive loss of the hydrogen. We suggest that the CO_2 may be the result of the same process but with carbon bonding with the oxygen. Volatiles such as CO_2 are easily trapped in deposits with small numbers of molecules in amorphous water ice (which condenses below 120 K) and are found in comets and interstellar grains (*16*, *17*). They also could be trapped in water-ice clathrate crystal structures, which form at temperatures above 120 K (*18*). Using these spectra (Fig. 1), we cannot distinguish among the several materials in which, and the different methods by which, such deposits of a few molecules could be trapped.

Alternative explanations for the material causing the 4.25-μm absorption include sulfur-bearing minerals, which sometimes show a fundamental stretch absorption at about 8.5 μm and might have a harmonic at 4.25 μm (*9*). However, in many cases there are other absorptions present that are not seen in the NIMS spectra. A few minerals, such as beryl and cordierite, sometimes exhibit 4.25-μm absorptions, but these minerals also have crystal structures that are known to trap volatiles. For example, trapped CO_2 has been suggested (*19*) to explain the absorptions in these minerals.

There are few candidates that might produce the 4.57-μm absorption in the spectra (Fig. 1). Although there are many organic molecules with absorptions in this range, most have additional features that are not present in the NIMS data. One candidate is the C≡N structural group, whose fundamental stretching absorption lies in the range 4.35 to 4.7 μm, with the exact location dependent on the molecule or molecules attached to CN. However, CN alone (or more naturally as HCN) absorbs at a wavelength shorter than 4.5 μm. Some tholins (Fig. 2B) (*20*) have absorptions near 4.57 μm with the appropriate band shapes that match the NIMS spectra. Further, there are no other features in these tholin spectra that disagree with the NIMS data. Tholins are the organic residue formed by subjecting mixtures (*21*) of simple C-, H-, O-, and N-bearing molecules to electrical discharge currents. The chemical composition of the resulting tholins is not completely characterized (*22*), but the triple-bonded CN species is most likely the spectrally active component (*20*). Another possibility is that the CN vibration causing the 4.57-μm absorption in the NIMS spectra is from cyanogen $(CN)_2$. This is a gas at room temperature and pressure (*23*) and could, as in the case of CO_2, be trapped in deposits of a few molecules to produce the observed spectra. Carbon monoxide also has a major absorption in this region and might be considered a likely candidate associated with the CO_2. However, the CO absorption is at about 4.67 μm, too long to match the NIMS spectra, and all variations of the CO band position for mixtures and clathrates known to us move the absorption to even

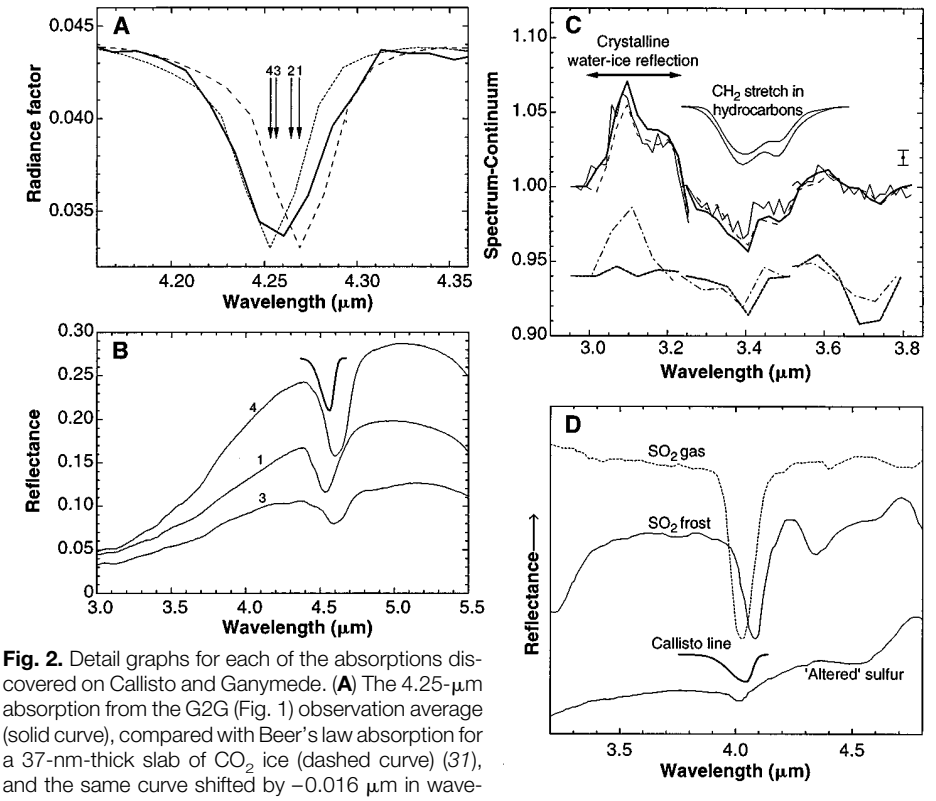

Fig. 2. Detail graphs for each of the absorptions discovered on Callisto and Ganymede. (**A**) The 4.25-μm absorption from the G2G (Fig. 1) observation average (solid curve), compared with Beer's law absorption for a 37-nm-thick slab of CO_2 ice (dashed curve) (*31*), and the same curve shifted by −0.016 μm in wavelength (dotted curve). Three of the numbered arrows mark the centers of the ν_3 absorption band for several forms of CO_2 ice (*32*): (1) amorphous, (2) crystalline, and (3) dispersed in a solid N_2 matrix at 10 K. The absorption center measured for Callisto is (4). (**B**) The model profile for the Callisto 4.57-μm absorption compared with the reflectance spectra of three tholins (*20, 21*) that show similar absorption features. (**C**) Five average Callisto spectra, including G2G (thin solid line, same data as used for Fig. 1), C3G (thin dashed line, same data as used for Fig. 1), C3A (heavy solid line in the top set of curves, same data as used for Fig. 1), C3-ASGARD (thin dot-dashed line, 5000 pixels from a regional area of 4000 km^2), and C3-CRATER (heavy dotted line in the bottom set of curves, 1800 pixels from a local 106 km^2 area). All averages have had a cubic-spline continuum removed from the displayed wavelength region. The first three averages show repeatable behavior, both in the 3.1-μm water ice reflection feature (indicated at the top) and in the 3.4-μm CH absorption. The two other observation averages have weaker features and are shown with a −0.06 offset. The absorption of two compounds with strong CH_2 absorptions (*26*) are shown in thin solid curves above the observations. The error bar indicates the maximum 1σ uncertainty among the displayed data due to nonsystematic sources. (**D**) Reflectance spectra on an arbitrary scale for three forms of SO_2 compared with the profile of the 4.05-μm absorption feature for Callisto. The SO_2 gas, SO_2 frost, and the preparation of the "altered" sulfur sample are described in (*28*).

longer wavelengths (*24*). Also, being smaller and considerably more volatile than CO_2, and tending to react with OH to produce CO_2 and H, CO is likely to be lost or eliminated from the surface (*25*).

Many CN-bearing molecules also contain CH components and C–H stretching transitions are responsible for absorptions in the 3.4-μm spectral region. There are no strong CH stretch absorptions in the NIMS data (Fig. 1), so molecules containing CH cannot be abundant, or at least not spectrally active. This is also true for the tholin spectra, which show only a slight feature at 3.4 μm. An average spectrum was calculated for each of five Callisto data sets, which revealed a feature at 3.4 μm in all of these average spectra (Fig. 2C). The feature is also present in the Ganymede spectra but is weaker than for Callisto. Three of the Callisto data sets produced nearly identical spectra after the continuum was removed (Fig. 2C), indicating that the feature is not due to noise. Error analysis performed on the NIMS spectra indicates that the uncertainty in the average spectrum due to nonsystematic sources is slightly larger than the line thickness in Fig. 2C. The shape of the 3.4-μm feature indicates a double band, with the longer wavelength feature being weaker. This is characteristic of the CH_2 stretch in aliphatic hydrocarbons, as illustrated by the plot of spectra for two CH_2-rich materials (*26*). The tholin spectra show a weak absorption similar to that shown for Callisto (Fig. 2B), which is probably due to C–H in the tholins.

Although the repeatability of the 3.4-μm feature in the NIMS data for different measurements (Fig. 2D) indicates that it is not due to noise, there is the possibility that it is due to instrument contamination or calibration uncertainties. Analysis of the radiometric calibration target (RCT) measurements made during the first two orbits of the mission revealed that there are undulations in the emission spectrum of the RCT, after the nominal NIMS calibration spectrum is applied in this spectral region. The undulations vary somewhat from measurement to measurement, but they are not similar to the Callisto 3.4-μm feature (Fig. 2C) and are about half the size of the absorption. Further, the NIMS spectra of Io were examined for the 3.4-μm feature, but no feature similar to the Callisto 3.4-μm feature was found. However, there are several weak SO_2 frost features in this general spectral region, particularly one at 3.35 μm, making comparison difficult. Thus, the weak feature appears to be neither a calibration error nor due to instrument contamination.

Sulfure dioxide is a candidate for the NIMS 4.05-μm absorption because it is very near a strong SO_2 absorption (*27*, *28*) and recent evidence of SO_2 on Callisto was reported from ultraviolet (UV) spectra (*29*). A more difficult question is in what form is the SO_2 present. In a compilation of the spectra of SO_2 materials (*28*) (Fig. 2D), the position of the condensed phase absorption is a bit too long to match the 4.05-μm band, but spectra of adsorbed forms of the SO_2 gas seem to be a better match. Sulfur dioxide, like CO_2, is too volatile to remain on the surface of Callisto and Ganymede for geologic time, but it would be more stable trapped in H_2O, as was suggested above for CO_2. Again, a logical species (SO_2) present in deposits of a few molecules within the surface material is a candidate for explaining the NIMS 4.05-μm absorption.

In the 3.88-μm region, the most likely species causing the absorption seems to be the S–H bond. Colthup *et al.* (*10*) identified isolated absorptions in the 3.86- to 3.94-μm region among organic chemicals to arise from BH or SH stretch, with SH likely to be far more abundant on the Galilean satellites, on the basis of cosmochemical grounds. Such an isolated band occurs in mercaptan and thiophenols. Other candidates in this region, such as NH^+ and sulphonic and sulphinic acids, have either too broad or too detailed a spectrum in this region to match the NIMS absorption.

The presence of solar UV and particle radiation from the jovian magnetosphere assures some molecular disassociation in the surface materials of Ganymede and Callisto. This radiation could play a role in creating some or all of the molecules identified here, and, with carbon-bearing molecules present, will produce graphite, which could be responsible for darkening the surface material. Finally, it is interesting to note that the spectral features for all but the sulfur molecules found in the NIMS data also appear in the spectrum of interstellar ices (*17*). This may indicate that these materials and the processes forming them are common in the colder regions (temperatures less than ~120 K) of the solar system and the universe. Some meteorites also contain organics with CH spectral features similar to the NIMS 3.4-μm absorptions (*30*). This suggests that the organic molecules in particular, and perhaps the other molecules described here, may accumulate on the surface of the Galilean satellites from outside the Jupiter system.

REFERENCES AND NOTES

1. Special issue on the Galileo Orbiter Observations of Jupiter and Its Satellites, *Science* **274**, 377–403 (18 October 1996); J. D. Anderson, W. L. Sjogren, G. Schubert, *ibid.* **272**, 709 (1996); J. D. Anderson, E. L. Lau, W. L. Sjogren, G. Schubert, W. B. Moore, *Nature* **384**, 541 (1996); *ibid.* **387**, 264 (1997); *Science* **276**, 1236 (1997).
2. K. Watson, B. C. Murray, H. Brown, *Icarus* **1**, 361 (1963).
3. R. W. Carlson, P. R. Weissman, W. D. Smythe, J. C. Mahoney, the NIMS Science and Engineering Team, *Space Sci. Rev.* **60**, 457 (1992).
4. Early results of the entire NIMS investigation (satellites and Jupiter) were reported previously by R. Carlson *et al.*, *Science* **274**, 385 (1996).
5. Early results for Callisto and Ganymede were reported by T. B. McCord *et al.*, *Bull. Am. Astron. Soc.* **28**, 1138 (abstr.) (1996); T. B. McCord *et al.*, *Trans. Am. Geophys. Union* **77**, F445 (abstr.) (1996); T. B. McCord *et al.*, *ibid.* **78**, S2O2 (abstr.) (1997).
6. N. Ockman, *Adv. Phys.* **7**, 199 (1958); W. M. Irvine and J. B. Pollack, *Icarus* **8**, 324 (1968); P. V. Hobbs, *Ice Physics* (Clarendon, Oxford, 1974); S. G. Warren, *Appl. Opt.* **23**, 1206 (1984).
7. U. Fink and H. P. Larson, *Icarus* **24**, 411 (1975).
8. C. B. Pilcher, S. T. Ridgway, T. B. McCord, *Science* **178**, 1087 (1972); U. Fink, N. H. Dekkers, H. P. Larson, *Astrophys. J.* **179**, L155 (1973); J. B. Pollack *et al.*, *Icarus* **36**, 271 (1978); G. T. Sill and R. N. Clark, in *Satellites of Jupiter*, D. Morrison, Ed. (Univ. of Arizona Press, Tucson, 1982), pp. 174–212; R. N. Clark, F. P. Fanale, M. J. Gaffey, in *Satellites*, J. Burns and M. S. Matthews, Eds. (Univ. of Arizona Press, Tucson, 1986), pp. 437–491; T. L. Roush, J. B. Pollack, F. C. Witteborn, J. D. Bregman, J. P. Simpson, *Icarus* **86**, 355 (1990); W. M. Calvin and R. N. Clark, *ibid.* **89**, 305 (1991); W. M. Calvin, R. N. Clark, R. H. Brown, J. R. Spencer, *J. Geophys. Res.* **100**, 19041 (1995).
9. For spectra of minerals, see R. N. Clark, the *USGS Digital Spectral Library 0.2-150 μm*, in preparation [see R. N. Clark, G. A. Swayze, A. Gallagher, T. V. V. King, W. M. Calvin, *U.S. Geol. Surv. Open File Rep. 93-592* (1993) for 0.2 to 3.0 μm]; J. W. Salisbury, L. S. Walter, N. Vergo, D. M. D'Aria, *Infrared (2.1–25 μm) Spectra of Minerals* (Johns Hopkins Univ. Press, Baltimore and London, 1991).
10. For spectra of organics, see N. B. Colthup, L. H. Daly, S. E. Wiberley, *Introduction to Infrared and Raman Spectroscopy* (Academic Press, San Diego, ed. 3, 1990).
11. For spectra of gaseous and frozen volatiles, see L. S. Rothman *et al.*, *J. Quant. Spectrosc. Radiat. Transfer* **48**, 469 (1992); U. Fink and G. T. Sill, in *Comets*, L. L. Wilkening, Ed. (Univ. of Arizona Press, Tucson, 1982), p. 164; R. H. Pierson, A. N. Fletcher, E. S. C. Glantz, *Anal. Chem.* **28**, 1218 (1956).
12. R. M. Goody and Y. L. Yung, in *Atmospheric Radiation* (Oxford Univ. Press, New York, ed. 2, 1989), pp. 67–124.
13. S. A. Sandford and L. J. Allamandola, *Astrophys. J.* **355**, 357 (1990).
14. R. E. Johnson and W. A. Jesser, *Astron. J.* **480**, L79 (1997); G. Notesco and A. Bar-Nun, *Icarus* **126**, 336 (1997).
15. J. R. Spencer, W. M. Calvin, J. Person, *J. Geophys. Res.* **100**, 19049 (1995); W. M. Calvin, R. E. Johnson, J. R. Spencer, *Geophys. Res. Lett.* **23**, 673 (1996); K. S. Noll, R. E. Johnson, A. L. Lane, D. L. Domingue, H. A. Weaver, *Science* **273**, 341 (1996).
16. A. H. Delsemme, in *Comets*, L. L. Wilkening, Ed. (Univ. of Arizona Press, Tucson, 1982), pp. 85–130.
17. D. C. B. Whittet *et al.*, *Astron. Astrophys.* **315**, L357 (1996).
18. D. Blake, L. Allamandola, S. Sandford, D. Hudgins, F. Freund, *Science* **254**, 548 (1991).
19. V. C. Farmer, *The Infrared Spectra of Minerals* (Mineralogical Society, London, 1974); E. F. Farrell and R. E. Newnham, *Am. Mineral.* **52**, 380 (1967); D. L. Wood and K. Nassau, *J. Chem. Phys.* **47**, 2220 (1967).
20. D. P. Cruikshank *et al.*, *Icarus* **94**, 345 (1991).
21. The initial gas mixtures are as follows: tholin 1, 50% CH_4 and 50% NH_3, plus small amounts of H_2O; tholin 3, 9% CH_4 and 91% N_2; and tholin 4, 90% N_2 and 10% CH_4.
22. For a description of the chemical analysis, see G. D. McDonald, B. N. Khare, W. R. Thompson, C. Sagan, *Icarus* **94**, 354 (1991).
23. At 150 K, cyanogen is a solid with a vapor pressure <0.1 mbar, almost identical to the behavior of SO_2.

24. S. A. Sandford and L. J. Allamandola, *Icarus* **76**, 201 (1988).
25. M. L. Delitsky and A. L. Lane, *J. Geophys. Res.* **102**, 16385 (1997).
26. *N*-Butyl sulfonal chloride (n-$C_4H_9SO_2Cl$) and *N*-nitroso piperidine ($C_5H_{10}N_2O$). Spectra are from (*10*).
27. W. D. Smythe, R. M. Nelson, D. B. Nash, *Nature* **280**, 766 (1979).
28. F. P. Fanale, R. H. Brown, D. P. Cruikshank, R. N. Clark, *ibid*., p. 761.
29. K. S. Noll, R. E. Johnson, M. A. McGrath, J. J. Caldwell, *Geophys. Res. Lett*. **24**, 1139 (1997).
30. J. L. Bishop, C. M. Pieters, T. Hiroi, *Meteoritics Planet. Sci*. **32**, A14 (1997).
31. S. G. Warren, *Appl. Opt.* **25**, 2650 (1986).
32. M. Falk, *J. Chem. Phys*. **86**, 560 (1987).

33. We acknowledge the use of the forthcoming U.S. Geological Survey 0.2-150 μm spectral library to be released by R.N.C. We thank D. Cruikshank for providing his published tholin spectra in digital form and D. Stevenson, J. Lunine, and many other colleagues for helpful discussions.

16 June 1997; accepted 2 September 1997

Inhibition of Hyperalgesia by Ablation of Lamina I Spinal Neurons Expressing the Substance P Receptor

Patrick W. Mantyh,* Scott D. Rogers, Prisca Honore, Brian J. Allen, Joseph R. Ghilardi, Jun Li, Randy S. Daughters, Douglas A. Lappi, Ronald G. Wiley, Donald A. Simone

Substance P is released in the spinal cord in response to painful stimuli, but its role in nociceptive signaling remains unclear. When a conjugate of substance P and the ribosome-inactivating protein saporin was infused into the spinal cord, it was internalized and cytotoxic to lamina I spinal cord neurons that express the substance P receptor. This treatment left responses to mild noxious stimuli unchanged, but markedly attenuated responses to highly noxious stimuli and mechanical and thermal hyperalgesia. Thus, lamina I spinal cord neurons that express the substance P receptor play a pivotal role in the transmission of highly noxious stimuli and the maintenance of hyperalgesia.

A subpopulation of dorsal root ganglion neurons synthesize (*1*) and transport (*2*) substance P (SP) to the spinal cord, where it is released upon noxious stimulation of the innervated peripheral tissue (*3*). Although SP excites spinal cord nociresponsive neurons (*4*), the role that SP and the substance P receptor (SPR) play in signaling nociceptive information remains unclear. In the normal animal, SP, upon release from primary afferents, diffuses to and interacts primarily with SPR-expressing neurons located in lamina I of the spinal cord (*5*–*7*). A high proportion of spinothalamic and spinobrachial neurons located in lamina I express SPR (*8*), suggesting that these SPR-expressing neurons play a role in the ascending conduction of nociceptive information.

To investigate the functions of lamina I SPR-expressing neurons in nociceptive signaling, we selectively ablated these neurons by infusing a cytotoxin conjugated to SP into the intrathecal space of the spinal cord in rats. When SP binds to spinal cord neurons expressing the SPR, both SP and SPR are rapidly internalized (*5*–*7*). Using SP-induced internalization of SPR as a specific portal of entry into SPR-expressing spinal cord neurons, we conjugated SP to the ribosome-inactivating protein saporin (SAP). This substance P–saporin conjugate (SP-SAP), like other saporin conjugates, must be internalized to exert its toxicity as it inactivates and ultimately kills cells by blocking protein synthesis (*9*). We performed a series of correlative in vitro and in vivo studies to determine the specificity and toxicity of SP-SAP, as well as functional changes in somatosensory processing.

Competition binding studies with ^{125}I-SP binding to membranes of the adult rat spinal cord demonstrated that SP-SAP [median inhibitory concentration (IC_{50}) = 2.2 nM] was nearly equipotent with SP (IC_{50} = 2.0 nM) in blocking the binding of ^{125}I-SP to the SPR (*10*), whereas neurokinin A (IC_{50} = 5 nM) was less potent, and SAP alone (1 μM) or the unrelated peptide endothelin-1 (1 μM) were totally inactive.

SP-SAP internalization and cytotoxicity were examined in primary cultures of neonatal rat spinal cord neurons (*11*), in which ~15% of the neurons express the SPR (*12*). Both SP (10^{-7} M) and SP-SAP (10^{-7} M) induced a rapid and similar extent of SPR

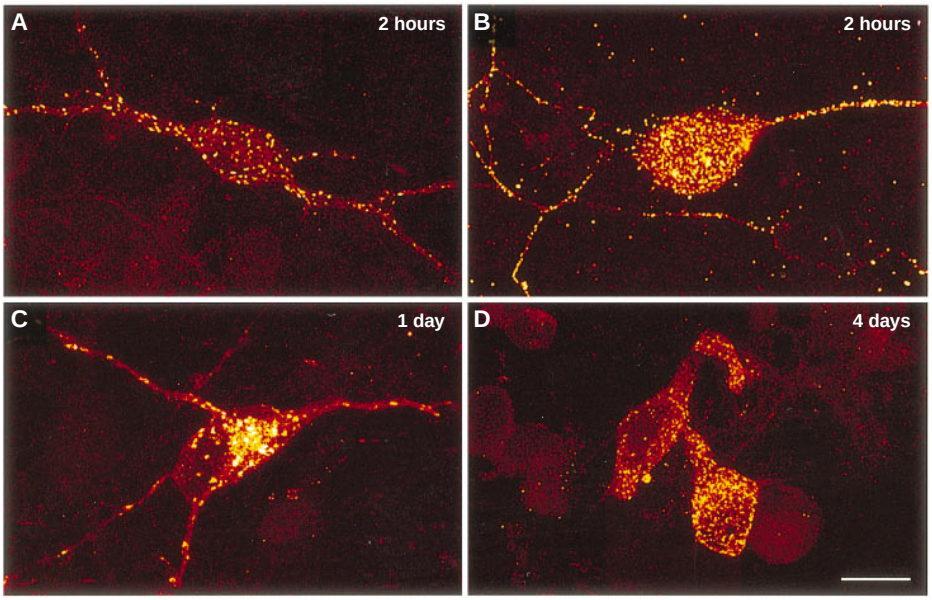

Fig. 1. Internalization and cytotoxicity of SP-SAP in primary cultures of neonatal spinal cord neurons (*11*). Confocal image of neurons where the SPR immunofluorescence (A, C, D) appears red, areas of concentrated SPR immunofluorescence appear yellow. (**A, C,** and **D**) SPR immunofluorescence in neurons 2 hours, 1 day, and 4 days, respectively, after treatment with SP-SAP. (**B**) Confocal image showing SAP immunofluorescence (yellow) 2 hours after SP-SAP treatment. These images were projected from 14 optical sections acquired at 0.8-μm intervals with a 60× lens. Bar, 25 μm.

P. W. Mantyh, S. D. Rogers, P. Honore, B. J. Allen, J. R. Ghilardi, Molecular Neurobiology Laboratory (151), Veterans Administration Medical Center, Minneapolis, MN 55417; and Department of Preventive Sciences, School of Dentistry, University of Minnesota and the Department of Psychiatry, University of Minnesota, Minneapolis, MN 55455, USA.
J. Li, R. S. Daughters, D. A. Simone, Department of Preventive Sciences, School of Dentistry, University of Minnesota and the Department of Psychiatry, University of Minnesota, Minneapolis, MN 55455, USA.
D. A. Lappi, Advanced Targeting Systems, 1600 Faraday Avenue, Carlsbad, CA 92008, USA.
R. G. Wiley, Neurology Service (147), Veterans Administration Medical Center, Nashville, TN 37212, USA.

*To whom correspondence should be addressed. E-mail: manty001@maroon.tc.umn.edu

Organics and Other Molecules in the Surfaces of Callisto and Ganymede

T. B. McCord, R. W. Carlson, W. D. Smythe, G. B. Hansen, R. N. Clark, C. A. Hibbitts, F. P. Fanale, J. C. Granahan, M. Segura, D. L. Matson, T. V. Johnson and P. D. Martin

Science **278** (5336), 271-275.
DOI: 10.1126/science.278.5336.271